14th International Conference on Structural Safety and Reliability - ICOSSAR'25
1-6 June, 2025 - Los Angeles California, USA
R. Ghanem, E. Johnson, S. Masri and A. Olivier (Eds)

OPTIMAL CUBIC NONLINEAR DAMPING FOR SEISMIC INTER-STORY VIBRATION ISOLATION UNDER CRITICAL DOUBLE AND MULTIPLE IMPULSE INPUTS

KOTARO KOJIMA[1], YUN-PENG ZHU[2] AND ZI-QIANG LANG[3]

[1]Faculty of Design and Architecture, Kyoto Institute of Technology
Matsugasaki, Sakyo-ku, Kyoto, 606-8585, Japan
kojima61@kit.ac.jp and https://researchmap.jp/kotarokojima?lang=en

[2]School of Engineering and Materials Science, Queen Mary University of London
Mile End Road, London E1 4NS, UK
yunpeng.zhu@qmul.ac.uk
https://www.sems.qmul.ac.uk/staff/y.zhu

[3]School of Electrical and Electronic Engineering, The University of Sheffield
Mappin Street, Sheffield, S1 3JD, UK
z.lang@sheffield.ac.uk
https://www.sheffield.ac.uk/eee/people/academic-staff/zi-qiang-lang

Key words: Cubic Nonlinear Damper, Vibration Isolation, Critical Earthquake Response, Double Impulse, Multiple impulse, Optimal Design.

Abstract. *Power-law nonlinear damping has been shown to be able to reduce the seismic responses of building structures over a broad range of frequencies. Many studies have been reported on the design of additional power law damping for the purpose of inter-story vibration isolation. The double and multiple impulse inputs were proposed to represent the near-fault and harmonic ground motions, respectively to facilitate a straightforward evaluation of the critical and resonant responses of elastic-plastic building systems to earthquake ground motions. In this study, a three-degree-of-freedom (3-dof) building system with a cubic nonlinear damper fitted on the second floor is considered. The nonlinear critical responses of this system to double and multiple impulse inputs with different amplitude levels are evaluated for the optimal design of the coefficient of the additional cubic damping. The optimal design is conducted based on the concept of Output Frequency Response Function (OFRF), which was derived by the frequency domain analysis of nonlinear systems and, in this study, allows the building response to the critical input to be represented as an explicit function of the damping coefficient to be designed. The objectives are to reduce the inter-story drift of each floor, the acceleration of the top floor, as well as the total vibration energy in critical cases of earthquake ground motions. The critical double and multiple impulse inputs have been defined as the inputs that can maximize the energy input into the system with their critical timing proven to be the timing when the sum of the inertial force of each floor becomes zero. The effectiveness of the optimally designed cubic damping is demonstrated using both recorded and simulated earthquake ground motions.*

1 INTRODUCTION

Power-law nonlinear damping has been shown to be able to reduce the seismic responses of building structures over a broad range of frequencies [1,2]. Many studies have been reported on the design of additional power-law damping for the purpose of inter-story vibration isolation under earthquake ground motions [3-6]. Lang et al. [3] proposed an iterative procedure for the optimal design of additional nonlinear damping. Zhu et al. [4] proposed a model synthesis method based on mobility analysis and linearization approaches for the design of nonlinearly damped building structures. Furthermore, Zhu et al. [5] expanded the proposed method in the previous study [4] to several simulated ground motions, and evaluated the effects of an optimal nonlinear viscous damper on minimizing the average sum of power of the inter-story drifts between different floors when building structures are subject to pulse-like ground motion excitations. Zhu et al. [6] reviewed the design theories of the nonlinear seismic isolation systems with nonlinear stiffness and additional nonlinear damping, including the above theories [1, 3, 4].

The Output Frequency Response Function (OFRF) representation of nonlinear systems is an extension of Frequency Response Function for linear systems to nonlinear cases [7]. The OFRF offers an explicit representation between system output spectra and nonlinear parameters to facilitate the design of nonlinear systems in the frequency domain [1-6].

Kojima and Takewaki [8, 9] proposed the double and multiple impulse inputs as the mathematical models for near-fault pulse-like earthquake ground motions and long-duration earthquake ground motions, respectively. The critical timing of these impulse inputs can be characterized by the zero restoring force timing for the single-degree-of-freedom system. Then, the closed-form and approximate closed-form solutions were derived for the critical double-impulse and multiple-impulse responses of the elastic-plastic system [8-11]. Akehashi and Takewaki [12] proved that the critical timing of the double impulse, which maximizes the energy input into the elastic-plastic multi-degree-of-freedom (MDOF) system, is the timing when the sum of the inertial forces of all masses becomes zero. Kawai and Takewaki [13] expanded this approach to the multiple impulse (MI) and defined the critical MI for the MDOF system as the MI in which each impulse acts when the sum of the inertial forces of all masses becomes zero.

In this paper, a three-degree-of-freedom (3-dof) building system with a cubic nonlinear damper fitted on the second floor is considered. The nonlinear critical responses of this system to double and multiple impulse inputs are evaluated. The critical double and multiple impulse inputs for the MDOF system have been defined as inputs that maximize the energy input into the system, and their critical timing is the timing when the sum of the inertial forces of all masses after the previous impulse becomes zero [12, 13]. Therefore, these critical timings can be easily captured for the nonlinear system, which changes depending on the nonlinear damping coefficient and input level. Then, the optimal coefficients of the additional cubic damping are obtained for the critical double and multiple impulse inputs with different input velocity amplitudes. The optimal design is conducted based on the concept of OFRF, which allows the building response to the critical input to be represented as an explicit function of the damping coefficient to be designed. The objectives are to reduce the inter-story drift of each floor, the acceleration of the top floor, as well as the total vibration energy in critical cases of earthquake ground motions. The effectiveness of the optimally designed cubic damping for the critical double and multiple impulse inputs is investigated using JMA Kobe NS component recorded during the Hyogo-ken Nanbu earthquake in 1995 and simulated earthquake ground motions.

2 THREE-DEGREE-OF-FREEDOM SYSTEM WITH CUBIC DAMPER

Consider a three-degree-of-freedom (3-dof) system with an additional cubic nonlinear damper fitted on the second floor as shown in Figure 1(a). m_1, m_2 and m_3 denote the masses of the second, third and rooftop floors, respectively, and $m_1 = m_2 = m_3 = 100 \times 10^3$ kg. k_i and c_i denote the shear stiffness and linear damping coefficient of the i-th story, and are set as follows.

$k_1 = 2.3687 \times 10^7$ N/m, $k_2 = 1.9739 \times 10^7$ N/m, $k_3 = 1.1844 \times 10^7$ N/m,

$c_1 = 1.5080 \times 10^5$ Ns/m, $c_2 = 1.2566 \times 10^5$ Ns/m, $c_3 = 7.5398 \times 10^4$ Ns/m.

The undamped fundamental natural period of this system is 1.0 s, and the stiffness distribution is set so that the shape of the fundamental mode is an inverted triangle distribution. The linear damping coefficients are set as the stiffness-proportional damping with a damping ratio of 2% for the fundamental mode. As shown in Figure 1(a), x_1, x_2, and x_3 are the displacements of the second, third, and rooftop floor masses relative to the ground (first floor), respectively, and $\ddot{x}_0$ denotes the ground acceleration. A dot on a variable denotes its time derivative. The inter-story drift of the i-th story is denoted by d_i, and $d_1 = x_1$, $d_2 = x_2 - x_1$ and $d_3 = x_3 - x_2$.

The damping force f_{non} of the additional cubic damper fitted between the second and third floors, whose damping force characteristic is shown in Figure 1(b), is expressed by [1-5]

$$f_{\text{non}} = c_{\text{non}} w(t)^3 , \tag{1}$$

where c_{non} (Ns^3/m^3) denotes the coefficient of the additional cubic damper, and $w(t) = \dot{x}_2 - \dot{x}_1$.

The equation of motion of this nonlinear system under the ground motion is expressed by

$$[\mathbf{M}]\{\ddot{\mathbf{x}}\} + [\mathbf{C}]\{\dot{\mathbf{x}}\} + \{\mathbf{f}_{\text{non}}\} + [\mathbf{K}]\{\mathbf{x}\} = -[\mathbf{M}]\{\mathbf{1}\}\ddot{x}_0 , \tag{2}$$

where $\{\mathbf{x}\}=\{x_1, x_2, x_3\}^{\mathrm{T}}$, $\{\mathbf{f}\}=\{-f_{\text{non}}, f_{\text{non}}, 0\}^{\mathrm{T}}$, $\{\mathbf{1}\} = \{1, 1, 1\}^{\mathrm{T}}$, and

$$[\mathbf{M}] = \begin{bmatrix} m_1 & & \\ & m_2 & \\ & & m_3 \end{bmatrix}, [\mathbf{C}] = \begin{bmatrix} c_1 + c_2 & -c_2 & \\ -c_2 & c_2 + c_3 & -c_3 \\ & -c_3 & c_3 \end{bmatrix}, [\mathbf{K}] = \begin{bmatrix} k_1 + k_2 & -k_2 & \\ -k_2 & k_2 + k_3 & -k_3 \\ & -k_3 & k_3 \end{bmatrix}.$$

3 DOUBLE AND MULTIPLE IMPULSE INPUTS

The double and multiple impulse inputs are employed as input ground motion models of near-fault pulse-like and long-duration ground motions, respectively. The ground acceleration modeled by the double impulse (DI) and multiple impulse (MI), as shown in Figures 2(a), (b), can be expressed as Equations (3) and (4) [8-14].

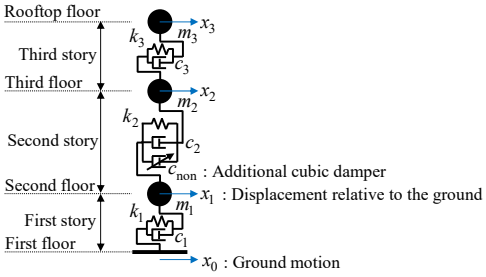

(a) 3-dof system with nonlinear damper

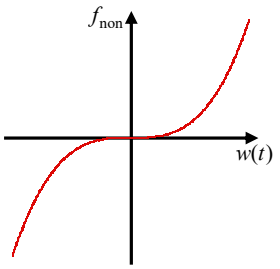

(b) f_{non}-w relation of cubic damper

Figure 1: 3-dof system with additional cubic nonlinear damper c_{non} fitted between second and third floors

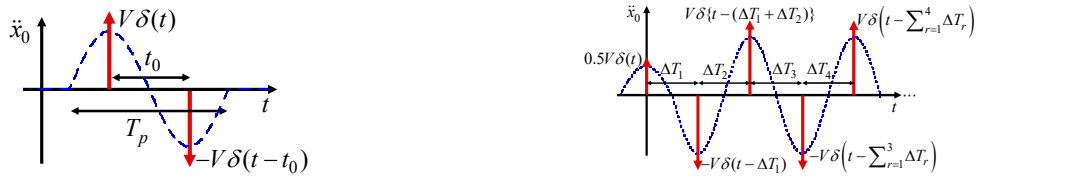

(a) Double impulse and one-cycle sine wave [8, 10, 12, 14] (b) Multiple impulse and multi-cycle sine wave [9, 13]

Figure 2: Double and multiple impulse inputs

$$\ddot{x}_0 = V\delta(t) - V\delta(t-t_0)\,, \tag{3}$$

$$\ddot{x}_0 = \frac{1}{2}V\delta(t) + \sum_{l=2}^{N-1}(-1)^{l-1}V\delta\left(t-\sum_{r=1}^{l-1}\Delta T_r\right) + (-1)^{N-1}\frac{1}{2}V\delta\left(t-\sum_{r=1}^{N-1}\Delta T_r\right), \tag{4}$$

where V denotes the given initial velocity by each impulse, t_0 denotes the time interval between the first and second impulses of the DI, ΔT_r is the time interval between the r-th and (r+1)-th impulses of the MI, N is the number of impulses of the MI, and $\delta(t)$ is the Dirac delta function. The initial velocities given by the first and last impulses of the MI are reduced to $0.5V$.

4 OPTIMAL CUBIC DAMPING UNDER CRITCAL DOUBLE IMPULSE

The critical double-impulse (DI) responses of the 3-dof system with a nonlinear damper are evaluated, and the relations between the critical DI responses and the nonlinear damper coefficients c_{non} are obtained. The critical timing t_0^{c} of the second impulse, which maximizes the input energy into this nonlinear system, is determined as the sum of the inertial forces of all masses becomes zero as follows [12]:

$$\{\mathbf{1}\}^{\text{T}}[\mathbf{M}]\{\ddot{\mathbf{x}}\} = 0\,. \tag{5}$$

Figures 3(a)-(c) show the relation between the maximum responses under the critical DI with the input velocity level V = 1.0 m/s, including the maximum inter-story drifts, maximum acceleration responses, maximum kinetic energy KE_i of each mass, maximum potential energy PE_i of the i-th floor and maximum total vibration energy $E_{\max}$, and the nonlinear cubic damper coefficient c_{non}. Figure 3(d) shows the critical timing t_0^{c}-c_{non} relation. The time-history response analyses are conducted for the nonlinear system to the DI, MI and ground motions using Newmark's method, and the unbalanced force of the nonlinear damping at the j step is released by applying it as an external force at the j+1 step. KE_i, PE_i and $E_{\max}$ are calculated by

$$KE_i = \max\left|\frac{1}{2}m_i\dot{x}_i^{\,2}\right|,\ PE_i = \max\left|\frac{1}{2}k_i d_i^{\,2}\right|, \tag{6, 7}$$

$$E_{\max} = \max\left|E(t)\right| = \max\left|\sum_{i=1}^{3}\frac{1}{2}m_i\dot{x}_i^{\,2} + \sum_{i=1}^{3}\frac{1}{2}k_i d_i^{\,2}\right|. \tag{8}$$

Furthermore, the energies, which mean the integrals of the squares of responses here, of the inter-story drift of the i-th story P_{di} and the rooftop floor acceleration P_{A3} are defined by [4, 5]

$$P_{di} = \int_0^\infty d_i^{\,2}\mathrm{d}t\,,\ P_{A3} = \int_0^\infty \ddot{x}_3^{\,2}\mathrm{d}t\,. \tag{9, 10}$$

In this paper, P_{di} and P_{A3} are calculated using the discrete-time $\ddot{x}_3$ and d_i, which are evaluated by the time-history response analysis (THRA), by

$$P_{di} = \sum_{j=1}^{LT} d_i(t_j)^2 \Delta t \,, \tag{11}$$

$$P_{A3} = \sum_{j=1}^{LT} \ddot{x}_3(t_j)^2 \Delta t \,, \tag{12}$$

where t_j (j = 1, 2, … LT) means the discrete time and LT denotes the number of data. The time increment $\Delta t = 10^{-4}$ s and $LT = 10^6+1$ (the time length for THRA is 100 s) for the critical DI.

P_{di}-c_{non} and P_{A3}-c_{non} relations are shown in Figures 3(e), (f), respectively. From Figure 3, the maximum inter-story drift of the third story, maximum acceleration at rooftop floor, $E_{\max}$, ΣP_{di} (= $P_{d1} + P_{d2} + P_{d3}$) and P_{A3} are minimized between $c_{\text{non}} = 10^7$-10^8 Ns^3/m^3.

The following three optimization problems (OPs) are considered, and these problems are solved using the concept of output frequency response function (OFRF) representation [4, 5, 7].

(OP1) Find c_{non} to minimize $\sum_{i=1}^{3} P_{di}$.

(OP2) Find c_{non} to minimize P_{A3}.

(OP3) Find c_{non} to minimize $E_{\max}$.

The output spectra of the inter-story drift $D_i(\mathrm{j}\omega)$ of the i-th story, the relative velocities $V_1(\mathrm{j}\omega)$, $V_2(\mathrm{j}\omega)$, $V_3(\mathrm{j}\omega)$ of the second, third and rooftop floor masses, and the rooftop floor acceleration $A_3(\mathrm{j}\omega)$ are expressed by the following OFRF representation as polynomial functions of the nonlinear damper coefficient c_{non} [4, 5, 7]:

$$D_i(\mathrm{j}\omega) = \sum_{n=0}^{N_{\max}} \lambda_{i,n}(\mathrm{j}\omega) {c_{\text{non}}}^n \,, \tag{13}$$

$$V_i(\mathrm{j}\omega) = \sum_{n=0}^{N_{\max}} \mu_{i,n}(\mathrm{j}\omega) {c_{\text{non}}}^n \,, \tag{14}$$

$$A_3(\mathrm{j}\omega) = \sum_{n=0}^{N_{\max}} \nu_n(\mathrm{j}\omega) {c_{\text{non}}}^n \,, \tag{15}$$

where $\lambda_{i,n}(\mathrm{j}\omega)$, $\mu_{i,n}(\mathrm{j}\omega)$, $\nu_n(\mathrm{j}\omega)$ and $N_{\max}$ denote the n-th order coefficients for $D_i(\mathrm{j}\omega)$, $V_i(\mathrm{j}\omega)$ and $A_3(\mathrm{j}\omega)$, and the maximum order of the OFRF representation, respectively. It is noted that the critical timing t_0^{c} of the DI changes as the nonlinear damping coefficient c_{non} becomes larger, as shown in Figure 3(d). In this paper, it is assumed that the output spectra $D_i(\mathrm{j}\omega)$, $V_i(\mathrm{j}\omega)$ and $A_3(\mathrm{j}\omega)$ can be expressed as Equations (13), (14), (15), even when the critical timing changes depending on c_{non}. The validity of this assumption needs to be investigated in the future.

From Equations (9), (10), (13) and (15), P_{di} and P_{A3} can be represented by the following OFRF representation.

$$P_{di} = \sum_{n=0}^{N_{\max}} \phi_{i,n} {c_{\text{non}}}^n \tag{16}$$

$$P_{A3} = \sum_{n=0}^{N_{\max}} \xi_n {c_{\text{non}}}^n \tag{17}$$

where $\phi_{i,n}$ and ξ_n denote the n-th order coefficients for P_{di} and P_{A3}, respectively.

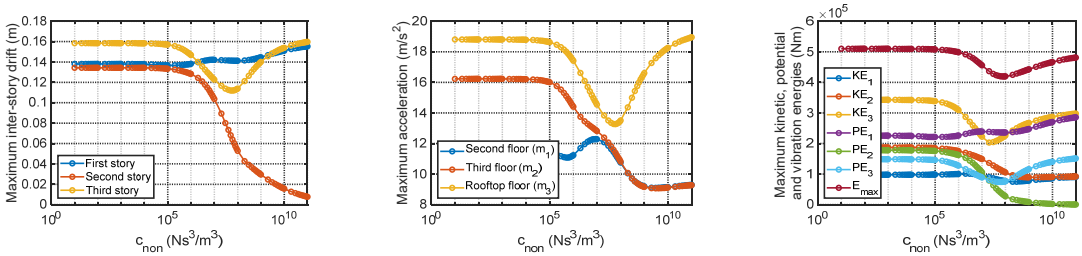

(a) Maximum inter-story drift (b) Maximum acceleration (c) KE_i, PE_i and $E_{\max}$

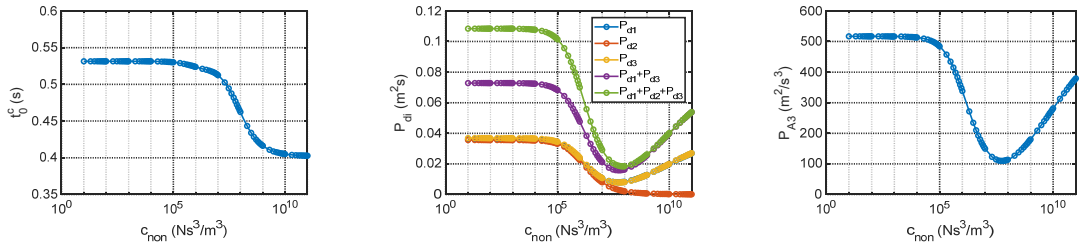

(d) Critical timing (e) P_{di} (f) P_{A3}

Figure 3: Critical double-impulse responses with respect to cubic damper coefficient

From Equations (13), (14) and (8), the OFRF representation of $E_{\max}$ is expressed by

$$E_{\max} = \sum_{n=0}^{N_{\max}} \psi_n c_{\text{non}}{}^n . \tag{18}$$

where ψ_n denote the n-th order coefficients for $E_{\max}$.

When P_{di}, P_{A3} and $E_{\max}$ are calculated for the 3-dof system with the different nonlinear damping coefficients $c_{\text{non},1}$, $c_{\text{non},2}$, … c_{non,N_c} under the critical double impulse, the following equations can be obtained from Equations (16)-(18).

$$\{\mathbf{P}_{di}\} = [\mathbf{C}_{\text{non}}]\{\mathbf{\Phi}_i\} \tag{19}$$

$$\{\mathbf{P}_{A3}\} = [\mathbf{C}_{\text{non}}]\{\mathbf{\Xi}\} \tag{20}$$

$$\{\mathbf{E}_{\max}\} = [\mathbf{C}_{\text{non}}]\{\mathbf{\Psi}\} \tag{21}$$

where $\{\mathbf{P}_{di}\} = \{P_{di,1}, P_{di,2}, \ldots P_{di,N_c}\}^{\mathrm{T}}$, $\{\mathbf{P}_{A3}\} = \{P_{A3,1}, P_{A3,2}, \ldots P_{A3,N_c}\}^{\mathrm{T}}$, $\{\mathbf{E}_{\max}\} = \{E_{\max,1}, E_{\max,2}, \ldots E_{\max,N_c}\}^{\mathrm{T}}$ are the vectors of P_{di}, P_{A3} and $E_{\max}$ for the different nonlinear damping coefficients $c_{\text{non},1}$, $c_{\text{non},2}$, … c_{non,N_c}, and $\{\mathbf{\Phi}_i\} = \{\phi_{i,0}, \phi_{i,1}, \ldots \phi_{i,N_{\max}}\}^{\mathrm{T}}$, $\{\mathbf{\Xi}\} = \{\xi_0, \xi_1, \ldots \xi_{N_{\max}}\}^{\mathrm{T}}$, $\{\mathbf{\Psi}\} = \{\psi_0, \psi_1, \ldots \psi_{N_{\max}}\}^{\mathrm{T}}$ are the vectors of the coefficients, respectively. $[\mathbf{C}_{\text{non}}]$ can be obtained as follows:

$$[\mathbf{C}_{\text{non}}] = \begin{bmatrix} 1 & c_{\text{non},1} & c_{\text{non},1}{}^2 & \cdots & c_{\text{non},1}{}^{N_{\max}} \\ \vdots & & \ddots & & \vdots \\ 1 & c_{\text{non},N_c} & c_{\text{non},N_c}{}^2 & \cdots & c_{\text{non},N_c}{}^{N_{\max}} \end{bmatrix} \tag{22}$$

The coefficients $\phi_{i,n}$, ξ_n and ψ_n can be obtained by the least squares method as follows [4, 5]:

$$\{\boldsymbol{\Phi}_i\} = \left([\mathbf{C}_{\text{non}}]^{\text{T}}[\mathbf{C}_{\text{non}}]\right)^{-1}[\mathbf{C}_{\text{non}}]^{\text{T}}\{\mathbf{P}_{di}\} \tag{23}$$

$$\{\boldsymbol{\Xi}\} = \left([\mathbf{C}_{\text{non}}]^{\text{T}}[\mathbf{C}_{\text{non}}]\right)^{-1}[\mathbf{C}_{\text{non}}]^{\text{T}}\{\mathbf{P}_{A3}\} \tag{24}$$

$$\{\boldsymbol{\Psi}\} = \left([\mathbf{C}_{\text{non}}]^{\text{T}}[\mathbf{C}_{\text{non}}]\right)^{-1}[\mathbf{C}_{\text{non}}]^{\text{T}}\{\mathbf{E}_{\max}\} \tag{25}$$

Figures 4(a)-(c) show comparisons of the THRA results of ΣP_{di}, P_{A3}, $E_{\max}$ under the critical DI input with $V = 1.0$ m/s for $c_{\text{non}} = 1.0 \times 10^7$, 1.5×10^7, … , 1.0×10^8 Ns^3/m^3, where $N_c = 19$, and the OFRF representation with $N_{\max} = 10$ evaluated from these THRA results. The optimal nonlinear damper coefficient subject to $c_{\text{non}} \in [10^7, 10^8]$, which is determined from Figure 3 for $V = 1.0$ m/s, evaluated based on the OFRF representation. The optimal c_{non} in the OP1, OP2 and OP3 for the critical DI with $V = 1.0$ m/s are 8.338×10^7, 5.566×10^7 and 7.996×10^7 Ns^3/m^3.

Figure 5(a) shows the optimal nonlinear damping coefficient for the different velocity amplitudes of the DI, $V = 0.5$, 1.0, 1.5, 1.756, 2.0, 2.5 m/s. $V = 1.756$ m/s is the velocity amplitude of the DI equivalent to JMA Kobe NS evaluated based on the reference [14] for the natural period of 1.0 s and the damping ratio of 2%. The constraint conditions of c_{non} need to be changed according to V, and are $c_{\text{non}} \in [10^8, 10^9]$ for $V = 0.5$ m/s, $c_{\text{non}} \in [10^7, 10^8]$ for $V = 1.0$, 1.5, 1.756 m/s, $c_{\text{non}} \in [5\times10^6, 5\times10^7]$ for $V = 2.0$ and 2.5 m/s, respectively. From Figure 5(a), the optimal c_{non} becomes smaller as the input velocity amplitude V is larger.

Figure 6 shows the inter-story drifts and relative acceleration responses under the critical DI with $V = 1.0$ m/s for $c_{\text{non}} = 0$ and 5.566×10^7 Ns^3/m^3, which is the optimal c_{non} for the OP2.

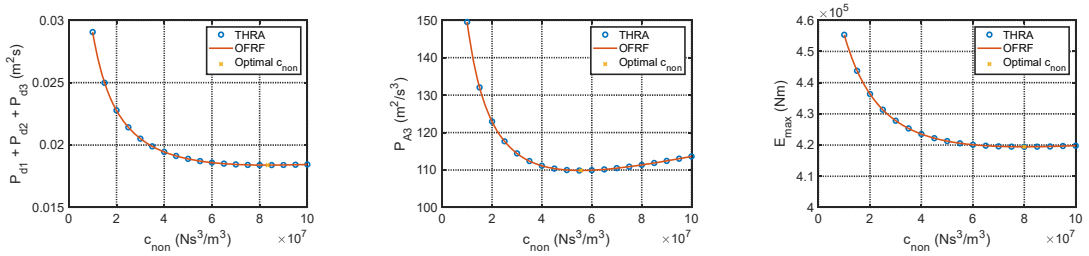

(a) ΣP_{di} (=$P_{d1} + P_{d2} + P_{d3}$) (b) P_{A3} (c) $E_{\max}$

Figure 4: OFRF representation for critical double-impulse responses and optimal c_{non}

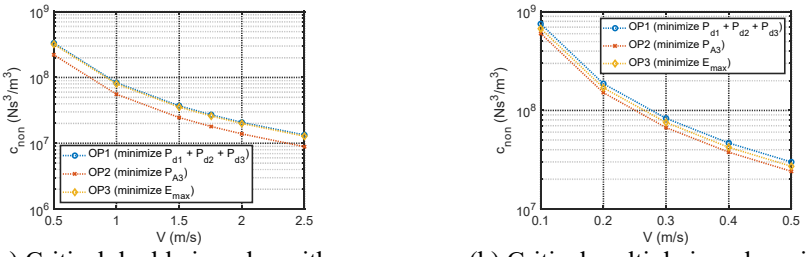

(a) Critical double impulse with $V = 0.5$, 1.0, 1.5, 1.756, 2.0, 2.5 m/s

(b) Critical multiple impulse with $V = 0.1$, 0.2, 0.3, 0.4, 0.5 m/s

Figure 5: Optimal cubic damper coefficient for critical double and multiple impulse inputs with different V

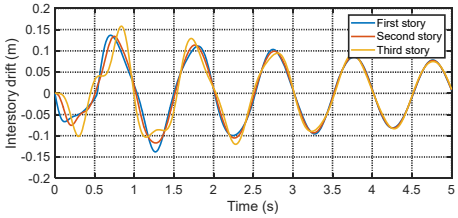

(a) Inter-story drift (c_{non} = 0 Ns^3/m^3)

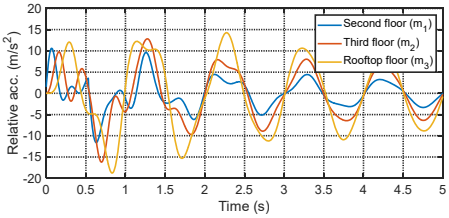

(b) Relative acceleration (c_{non} = 0 Ns^3/m^3)

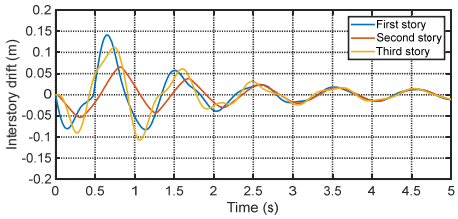

(c) Inter-story drift (c_{non} = 5.566 × 10^7 Ns^3/m^3)

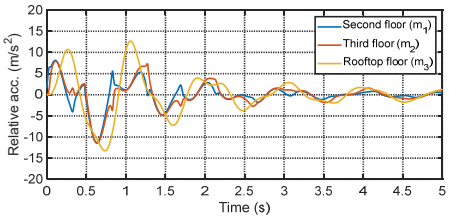

(d) Relative acceleration (c_{non} = 5.566 × 10^7 Ns^3/m^3)

Figure 6: Critical double-impulse responses for V = 1.0 m/s and c_{non} = 0, 5.566 × 10^7 Ns^3/m^3

5 OPTIMAL CUBIC DAMPING UNDER CRITCAL MULTIPLE IMPULSE

The critical nonlinear responses of the 3-dof system under the multiple impulse (MI) are evaluated, and the relations between the critical MI responses and the cubic damper coefficients c_{non} are obtained. Figures 7(a)-(c) show the relation between the maximum responses under the critical MI with V = 0.2 m/s and c_{non}. As defined in the reference [13], the timing of each impulse of the critical MI is determined as the timing when the sum of the inertial forces of all masses after the previous impulse becomes zero, as shown in Equation (5). The number of impulses N is set to 200 to converge the critical response to the steady state. Figure 7(d) shows the relation between the critical timing ΔT^e and c_{non} after the critical MI response converges to the steady state. The energy of inter-story drift P_{di} and that of rooftop floor acceleration P_{A3} are also calculated, and shown in Figures 7(e), (f) for the different c_{non}. In section 5, the time increment Δt = 10^{-4} s, LT = 2×10^6+1 and the time length for the THRA is 200 s. From Figures 7(c), (e), (f), E_{max}, ΣP_{di} (= P_{d1} + P_{d2} + P_{d3}) and P_{A3} are minimized between c_{non} = 5×10^7-5×10^8 Ns^3/m^3.

The optimal c_{non} for the critical MI is evaluated by a similar procedure in section 4 using the concept of the OFRF representation [4, 5, 7] in the OP1-OP3. Figures 8(a)-(c) show the THRA results of ΣP_{di}, P_{A3} and E_{max} under the critical MI with V = 0.2 m/s for c_{non} = 5.0 × 10^7, 7.5 × 10^7, … , 5.0 × 10^8 Ns^3/m^3 and their OFRF representation. The optimal c_{non} subject to the constrain condition $c_{non} \in \left[5\times10^7, 5\times10^8\right]$, which is determined from Figure 7, are 1.866×10^8, 1.513×10^8 and 1.694×10^8 Ns^3/m^3 in the OP1, OP2 and OP3 for the critical MI with V = 0.2 m/s based on the OFRF representation. Figure 5(b) shows the optimal nonlinear damping coefficient for the different velocity amplitudes, V = 0.1, 0.2, 0.3, 0.4, 0.5 m/s. The constraint conditions of c_{non} need to be changed depending on V, and are $c_{non} \in \left[10^8, 10^9\right]$ for V = 0.1 m/s, $c_{non} \in \left[5\times10^7, 5\times10^8\right]$ for V = 0.2 m/s, $c_{non} \in \left[10^7, 10^8\right]$ for V= 0.3, 0.4, 0.5 m/s, respectively.

Figure 9 shows d_i and $\ddot{x}_i$ under the critical MI with V = 0.2 m/s for c_{non} = 0, 1.866 × 10^8 Ns^3/m^3. 1.866 × 10^8 Ns^3/m^3 are the optimal c_{non} in the OP1 for the critical MI with V = 0.2 m/s.

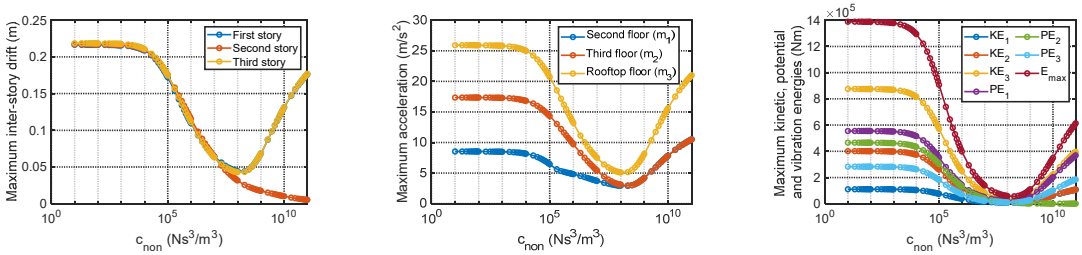

(a) Maximum inter-story drift (b) Maximum acceleration (c) KE_i, PE_i and $E_{\max}$

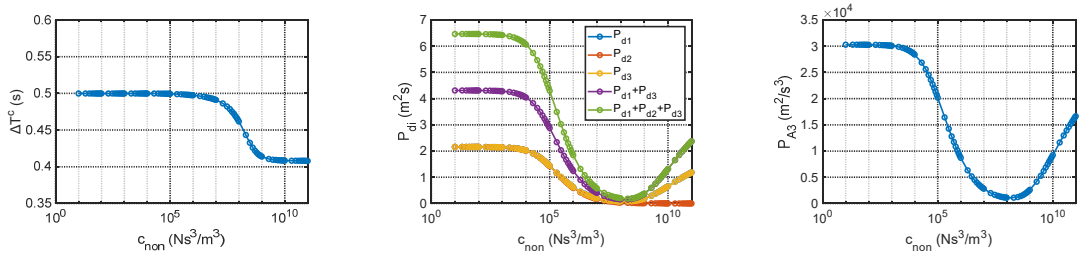

(d) Critical timing (e) P_{di} (f) P_{A3}

Figure 7: Critical multiple-impulse responses with respect to cubic damper coefficient

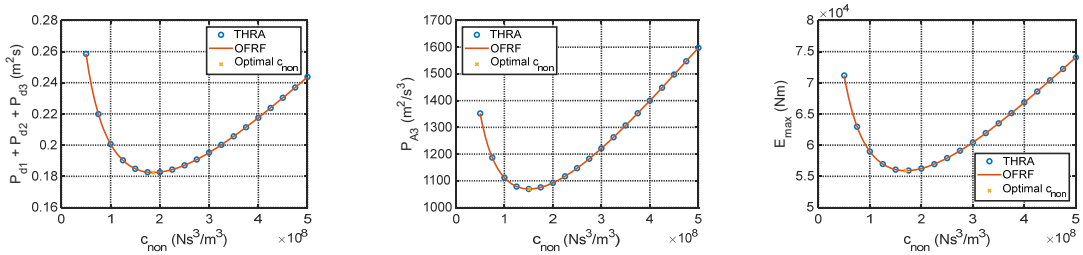

(a) ΣP_{di} (=$P_{d1} + P_{d2} + P_{d3}$) (b) P_{A3} (c) $E_{\max}$

Figure 8: OFRF representation for critical multiple-impulse responses and optimal cubic damper coefficient

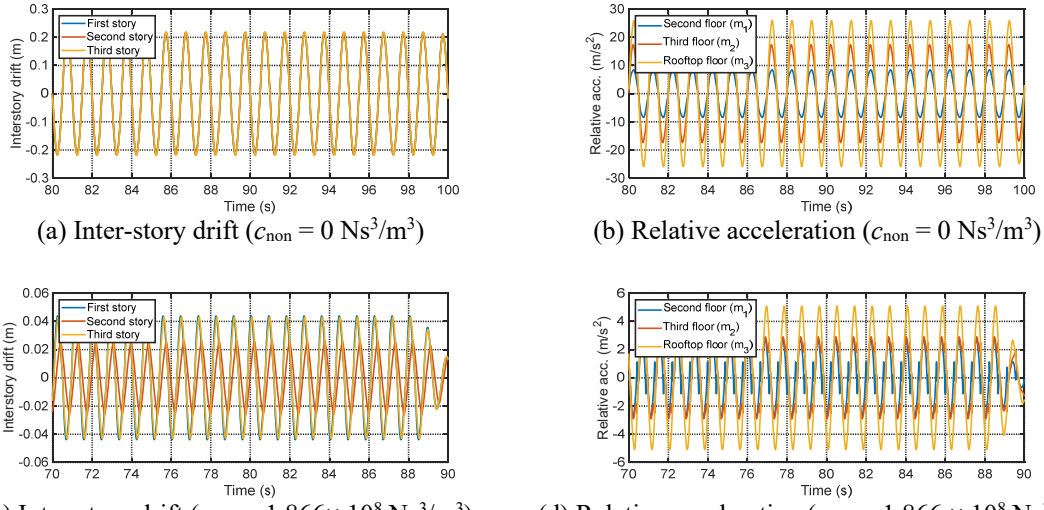

(a) Inter-story drift (c_{non} = 0 Ns^3/m^3) (b) Relative acceleration (c_{non} = 0 Ns^3/m^3)

(c) Inter-story drift (c_{non} = 1.866× 10^8 Ns^3/m^3) (d) Relative acceleration (c_{non} = 1.866 × 10^8 Ns^3/m^3)

Figure 9: Critical MI responses for V = 0.2 m/s and c_{non} = 0 and 1.866 × 10^7 Ns^3/m^3

6 EFFICIENCY INVESTIGATION THROUGH COMPARISON WITH ACTUAL AND SIMULATED GROUND MOTIONS

To investigate the efficiency of the optimal nonlinear damping c_{non} evaluated for the critical DI and MI inputs, the responses of the 3-dof system with optimal nonlinear damper and without nonlinear damper are compared under the JMA Kobe NS component and two simulated earthquake ground motions with random phases which are compatible to the safety-limit level design response spectrum at the engineering bedrock surface in the seismic design code in Japan [15], as shown in Figure 10. P_{A3} under the ground motions is defined as the energy of the absolute acceleration of the rooftop floor and calculated by

$$P_{A3} = \sum_{j=1}^{LT} \left\{ \ddot{x}_3(t_j) + \ddot{x}_0(t_j) \right\}^2 \Delta t \,. \tag{26}$$

The optimal c_{non} for the critical DI with $V = 1.756$ m/s are 2.711×10^7, 1.799×10^7 and 2.595×10^7 Ns^3/m^3 in the OP1, OP2, OP3, respectively, as shown in Figure 5(a). ΣP_{di}, P_{A3} and E_{max} of the 3-dof system with the optimal $c_{non} = 2.711 \times 10^7$, 1.799×10^7, 2.595×10^7 Ns^3/m^3 under JMA Kobe NS and their reduction rates from those without a nonlinear damper are summarized in Table 1. The results for the optimal c_{non} in the OP1 and OP2 with $V = 1.0$, and 2.0 m/s are also shown in Table 1. ΣP_{di} for $c_{non} = 2.711 \times 10^7$ Ns^3/m^3 and P_{A3} for $c_{non} = 1.799 \times 10^7$ Ns^3/m^3 are reduced to about 19% and 25%, respectively, from the system without a nonlinear damper.

The efficiency of the optimal c_{non} for the critical MI with $V = 0.1$ and 0.2 m/s are investigated through the comparison of the responses of the 3-dof system with optimal nonlinear damper and without the nonlinear damper under the simulated earthquake ground motions (EQGMs) with the time durations $t_d = 60$ s and 120s, as shown in Figure 10. As shown in Figure 5(b), the optimal c_{non} in the OP1-OP3 for the critical MI with $V = 0.1$ m/s are 7.530×10^8, 6.027×10^8 and 6.745×10^8 Ns^3/m^3, respectively. And these for $V = 0.2$ m/s are 1.866×10^8, 1.513×10^8 and 1.694×10^8 Ns^3/m^3, respectively. Tables 2 and 3 show ΣP_{di}, P_{A3}, E_{max} and those reduction

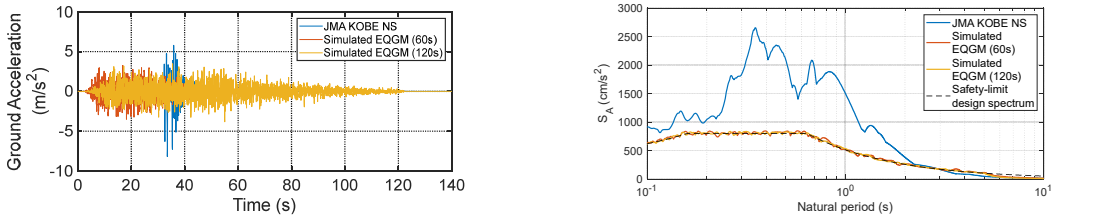

(a) Ground accelerations (b) Acceleration response spectra (damping ratio: 5%)

Figure 10: Input earthquake ground motions (EQGMs) and their acceleration response spectra

Table 1: ΣP_{di}, P_{A3} and E_{max} to JMA Kobe NS for optimal c_{non} based on OFRF representation for critical DI

C_{non} (Ns^3/m^3)	V (m/s), OP	ΣP_{di} (m^{2}s)	P_{A3} (m^2/s^3)	E_{max} (Nm)	Reduction rate of ΣP_{di}	Reduction rate of P_{A3}	Reduction rate of E_{max}
0		0.3319	1601	10.23×10^5			
1.799×10^7	1.756, OP2	0.0654	398	7.06×10^5	19.7%	24.8%	69.0%
2.595×10^7	1.756, OP3	0.0626	393	6.90×10^5	18.9%	24.5%	67.5%
2.711×10^7	1.756, OP1	0.0624	393	6.88×10^5	18.8%	24.5%	67.3%
8.338×10^7	1.0, OP1	0.0615	419	6.75×10^5	18.5%	26.1%	66.0%
5.566×10^7	1.0, OP2	0.0608	404	6.74×10^5	18.3%	25.2%	65.9%
2.078×10^7	2.0, OP1	0.0641	395	6.99×10^5	19.3%	24.7%	68.4%
1.389×10^7	2.0, OP2	0.0684	406	7.20×10^5	20.6%	25.4%	70.4%

rates of the system with c_{non} = 7.530 × 10^8, 6.027 × 10^8, 1.866 × 10^8, 1.513 × 10^8 Ns^3/m^3 under the two simulated EQGMs. From Table 2, ΣP_{di} and P_{A3} of the system with c_{non} = 7.530 × 10^8 and 6.027 × 10^8 Ns^3/m^3 under the simulated EQGM with t_d = 60 s are reduced to about 17 % and about 24 % from the system without a nonlinear damper, respectively. From Table 3, ΣP_{di} for c_{non} = 7.530 × 10^8 Ns^3/m^3 under the simulated EQGM with t_d = 120 s is reduced to about 32 %, and P_{A3} for c_{non} = 6.027 × 10^8 Ns^3/m^3 is reduced to about 43 %.

7 CONCLUSIONS

The nonlinear critical responses were evaluated for a three-degree-of-freedom building system with an additional cubic nonlinear damper fitted between the second and third floors under double and multiple impulse inputs. Furthermore, the optimal damping coefficients of the additional cubic damper were obtained to minimize the energies of inter-story drifts and rooftop floor acceleration, which are the integrals of the squares of these responses, and the maximum vibration energy, which is the maximum value of the sum of all potential and kinetic energies, under the critical double and multiple impulse inputs using the concept of the output frequency response function (OFRF). The effectiveness of the optimally designed cubic damping was investigated using JMA Kobe NS and simulated ground motions. The sum of energies of inter-story drifts and the energy of rooftop floor acceleration under the JMA Kobe NS can be reduced to about 19-20% and 25%, respectively, by the optimal nonlinear damping for the critical double impulse with the input velocity level of 1.756 m/s. The sum of energies of inter-story drifts and the energy of rooftop floor acceleration under the two simulated ground motions can be reduced to about 17-32 % and 24-44 %, respectively, by the optimal nonlinear damping for the critical multiple impulse with the input velocity amplitude of 0.1 m/s.

ACKNOWLEDGEMENTS

This research is partially supported by KAKENHI of the Japan Society for the Promotion of Science (No. 23K13439). JMA KOBE was provided by the Japan Meteorological Agency. The authors are grateful to Mr. Takahiro Ohashi, a graduate student at the Graduate School of Science and Technology, Kyoto Institute of Technology, for making the simulated ground motions. These supports are greatly appreciated.

Table 2: Σ P_{di}, P_{A3} and E_{max} under Simulated EQGM (60 s) with optimal c_{non} based on OFRF for critical MI

C_{non} (Ns^3/m^3)	V (m/s), OP	ΣP_{di} (m^2s)	P_{A3} (m^2/s^3)	E_{max} (Nm)	Reduction rate of ΣP_{di}	Reduction rate of P_{A3}	Reduction rate of E_{max}
0		0.1352	648	17.28×10^4			
7.530×10^8	0.1, OP1	0.0234	154	6.02×10^4	17.3%	23.7%	34.8%
6.027×10^8	0.1, OP2	0.0236	152	5.66×10^4	17.4%	23.5%	32.8%
1.866×10^8	0.2, OP1	0.0270	158	5.06×10^4	20.0%	24.4%	29.3%
1.513×10^8	0.2, OP2	0.0281	162	5.18×10^4	20.8%	25.0%	30.0%

Table 3: Σ P_{di}, P_{A3} and E_{max} under Simulated EQGM (120 s) with optimal c_{non} based on OFRF for critical MI

C_{non} (Ns^3/m^3)	V (m/s), OP	ΣP_{di} (m^2s)	P_{A3} (m^2/s^3)	E_{max} (Nm)	Reduction rate of ΣP_{di}	Reduction rate of P_{A3}	Reduction rate of E_{max}
0		0.1168	574	13.79×10^4			
7.530×10^8	0.1, OP1	0.0376	251	5.60×10^4	32.2%	43.6%	40.6%
6.027×10^8	0.1, OP2	0.0378	247	5.35×10^4	32.4%	43.1%	38.8%
1.866×10^8	0.2, OP1	0.0424	251	5.48×10^4	36.3%	43.6%	39.7%
1.513×10^8	0.2, OP2	0.0439	255	5.74×10^4	37.6%	44.4%	41.6%

REFERENCES

[1] Lang, Z.Q., Jing, X.J., Billings, S.A., Tomlinson, G.R. and Peng, Z.K. Theoretical study of the effects of nonlinear viscous damping on vibration isolation of sdof systems. *J. Sound Vib.* (2009) **323**(1–2):352-365.

[2] Peng, Z.K., Lang, Z.Q., Zhao, L., Billings, S.A., Tomlinson, G.R. and Guo, P.F. The force transmissibility of MDOF structures with a non-linear viscous damping device. *Int. J. Non-Linear Mech.* (2011) **46**(10):1305-1314.

[3] Lang, Z.Q., Guo, P.F. and Takewaki, I. Output frequency response function based design of additional nonlinear viscous dampers for vibration control of multi-degree-of-freedom systems. *J. Sound Vib.* (2013) **332**(19):4461-4481.

[4] Zhu, Y.P., Lang, Z.Q., Fujita, K. and Takewaki, I. The design of nonlinear damped building isolation systems by using mobility analysis. *Front. Built Environ.* (2022) **8**:971260.

[5] Zhu, Y.P., Kojima, K., Lang, Z.Q. and Gao, B.Y. Dynamic sub-structuring based nonlinear damping design for building inter-story isolation systems. *Proc. SECED 2023 Conference*, *Earthq. Eng. Dyn. Sustainable Future*, 14-15 Sept. (2023), Cambridge, UK, ID: 220.

[6] Zhu, Y.P., Lang, Z.Q., Fujita, K. and Takewaki, I. Analysis and design of non-linear seismic isolation systems for building structures—An overview. *Front. Built Environ.* (2023) **8**:1084081.

[7] Lang, Z.Q., Billings, S.A., Yue, R. and Li, J. Output frequency response function of nonlinear Volterra systems. *Automatica* (2007) **43**(5):805-816.

[8] Kojima, K. and Takewaki, I. Critical earthquake response of elastic–plastic structures under near-fault ground motions (Part 1: Fling-step input). *Front. Built Environ.* (2015) **1**:12.

[9] Kojima, K. and Takewaki, I. Critical input and response of elastic–plastic structures under long-duration earthquake ground motions. *Front. Built Environ.* (2015) **1**:15.

[10] Kojima, K., Saotome, Y. and Takewaki, I. Critical earthquake response of a SDOF elastic-perfectly plastic model with viscous damping under double impulse as a substitute for near-fault ground motion. *Jpn. Archit. Rev.* (2018) **1**:207–220.

[11] Kojima, K. and Takewaki, I. Critical steady-state response of single-degree-of-freedom bilinear hysteretic system under multi impulse as substitute of long-duration ground motion. *Front. Built Environ.* (2017) **3**: 41.

[12] Akehashi, H. and Takewaki, I. Optimal viscous damper placement for elastic-plastic MDOF structures under critical double impulse. *Front. Built Environ.* (2019) **5**:20.

[13] Kawai, A. and Takewaki, I. Critical response of multi-story damped bilinear hysteretic shear building under multi impulse as representative of long-period, long-duration earthquake ground motions. *Front. Built Environ.* (2020) **6**:588980.

[14] Akehashi, H. and Takewaki, I. Bounding of earthquake response via critical double impulse for efficient optimal design of viscous dampers for elastic-plastic moment frames. *Jpn. Archit. Rev.* (2022) **5**(2):131–149.

[15] National Institute for Land and Infrastructure Management, Building Research Institute. *Commentary on structural regulations of the building standard law of Japan, 2020 edition*. Official Gazette Co-operation of Japan, (2020). (in Japanese)